THE JOURNAL OF BIOLOGICAL CHEMISTRY
Vol. 278, No. 18, Issue of May 2, pp. 16030–16038, 2003
Printed in U.S.A.

Low Resolution Structures of the Retinoid X Receptor DNA-binding and Ligand-binding Domains Revealed by Synchrotron X-ray Solution Scattering*

Received for publication, July 11, 2002, and in revised form, December 4, 2002
Published, JBC Papers in Press, January 17, 2003, DOI 10.1074/jbc.M206953200

Hannes Fischer‡§¶, Sandra M. G. Dias‡¶, Maria A. M. Santos‡, Adriana C. Alves‖, Nilson Zanchin‖, Aldo F. Craievich§, James W. Apriletti, John D. Baxter**‡‡, Paul Webb**, Francisco A. R. Neves§§, Ralff C. J. Ribeiro†§§, and Igor Polikarpov‡‖¶¶**

*From the ‡Instituto de Física de São Carlos, Universidade de São Paulo, Av. Trabalhador São Carlense, 400 São Carlos, SP, Brazil 13560-970, the §Instituto de Física, Universidade de São Paulo, São Paulo, SP, Brazil 05508-900, the ‖Laboratório Nacional de Luz Síncrotron, Campinas, SP, Brazil 13084-971, the **Diabetes Center, Metabolic Research Unit, and the Department of Medicine, University of California San Francisco, San Francisco, California 94143, and the §§Departamento de Ciências Farmacêuticas, Universidade de Brasília, Brasília, DF, Brazil 70900-910*

Nuclear receptors are ligand-inducible transcription factors that share structurally related DNA-binding (DBD) and ligand-binding (LBD) domains. Biochemical and structural studies have revealed the modular nature of DBD and LBD. Nevertheless, the domains function in concert *in vivo*. While high-resolution crystal structures of nuclear receptor DBDs and LBDs are available, there are no x-ray structural studies of nuclear receptor proteins containing multiple domains. We report the solution structures of the human retinoid X receptor DBD-LBD (hRXRαΔAB) region. We obtained *ab initio* shapes of hRXRαΔAB dimer and tetramer to 3.3 and 1.7 nm resolutions, respectively, and established the position and orientation of the DBD and LBD by fitting atomic coordinates of hRXRα DBD and LBD. The dimer is U-shaped with DBDs spaced at ~2 nm in a head to head orientation forming an angle of about 10° with respect to each other and with an extensive interface area provided by the LBD. The tetramer is a more elongated X-shaped molecule formed by two dimers in head to head arrangement in which the DBDs are extended from the structure and spaced at about 6 nm. The close proximity of DBDs in dimers may facilitate homodimer formation on DNA; however, for the homodimer to bind to a DNA element containing two directly repeated half-sites, one of the DBDs would need to rotate with respect to the other element. By contrast, the separation of DBDs in the tetramers may account for their decreased ability to recognize DNA.

The nuclear receptor gene family in humans consists of at least 48 structurally related proteins that regulate transcription of target genes (1). These include receptors for the steroid and thyroid hormones, retinoids, vitamin D, prostaglandins, fatty acids, and unknown ligands, the orphan receptors. Nuclear receptors are comprised of single polypeptide chains that contain modular domains (2–4). The N termini of the receptors, which are the most variable in length, have transcription transactivation functions. The centrally placed and highly conserved DNA-binding domain (DBD)[1] directs receptor binding to DNA and is also involved in dimerization. The carboxyl-terminal ligand-binding domain (LBD) binds the ligand and undergoes ligand-induced conformational changes that promote dissociation of corepressors and association of coactivators that mediate receptor-induced changes in transcriptional control. The LBD also participates in receptor homodimerization, heterodimerization, and oligomerization (5, 6).

Retinoids exert multiple effects on morphogenesis and differentiation in fetal and adult organs and regulate glucose and lipid homeostasis. They also act as potent inhibitors of oncogenesis in rodent models and are used as chemo-preventive and therapeutic agents in several types of cancers in humans (7–12). In mice retinoid X receptor (RXR) selective agonists function as insulin sensitizers and can decrease hyperglycemia, hypertriglyceridemia, and hyperinsulinemia (13). The three RXR isoforms (α, β, and γ) bind to 9-cis retinoic acid and can function either as homodimers or heterodimers with many other members of the nuclear receptor family, including the receptors for thyroid hormones (TRs), vitamin D, and the peroxisome proliferator-activated receptors. RXR homodimers bind preferentially to direct repeats (DRs) of the AGGTCA half-site spaced by one nucleotide (DR-1), whereas heterodimers with peroxisome proliferator-activated receptors, vitamin D receptors, TRs, and retinoic acid receptors bind to DRs spaced by 1, 3, 4, or 5 nucleotides, respectively.

The RXR has been reported to exist either as a mixed population of monomers, dimers, and tetramers (14) or monomers and tetramers (15) in solution. In the absence of ligand, the values for $K_{d\ \mathrm{monomer}\rightarrow\mathrm{dimer}}$ and $K_{d\ \mathrm{dimer}\rightarrow\mathrm{tetramer}}$ are 130 and 2.8 nM, respectively, as calculated from fluorescence anisotropy

* This work was supported by Conselho Nacional de Desenvolvimento Científico e Tecnológico (CNPq) Grants 333991-2 (to R. C. J. R.) and 300220/96-0) (to I. P.), Programa de Apoio ao Desenvolvimento Científico e Technologico Grant 333449-x (to R. C. J. R.), Fundação de Amparo à Pesquisa do Estado de São Paulo (FAPESP) Grants 99/03387-4, 00/00021-8, and 99/09471-7, and National Institutes of Health Grants DK41842 and DK09516 (to J. D. B.). The costs of publication of this article were defrayed in part by the payment of page charges. This article must therefore be hereby marked "*advertisement*" in accordance with 18 U.S.C. Section 1734 solely to indicate this fact.

† Deceased.

¶ Both authors contributed equally to this work.

‡‡ Has proprietary interests in, and serves as a consultant and Deputy Director to, Karo Bio AB, which has commercial interests in this area of research.

¶¶ To whom correspondence should be addressed: Dept. de Fisica e Informatica, Universidade de São Paulo, Av Trabalhador Sao Carlense 400, São Carlos, SP, Brazil 13560-970. Tel.: 55-16-273-8088; Fax: 55-16-273-9881; E-mail: IPolikarpov@if.sc.usp.br.

[1] The abbreviations used are: DBD, DNA-binding domain; LBD, ligand-binding domain; RXR, retinoid X receptor; TRs, thyroid receptors; DRs, direct repeats; SAXS, small-angle x-ray scattering; DTT, dithiothreitol; DAM, dummy atom model; CRBP, cellular retinol-binding protein.

titration studies, indicating that in this setting tetramer formation is favored (14). Addition of ligand to tetramers in solution leads to their rapid dissociation to form homodimers (14, 15). Moreover, unliganded RXR dimers bind DR-1 relatively strongly, but the tetramers do not. Addition of DR-1 DNA to tetramer-containing solutions leads to formation of dimers. Thus, both ligand and the RXR cognate DNA element shift the dynamic equilibrium between RXR tetramer and dimer so that dimer formation is enhanced.

A large number of isolated nuclear receptor DBD and LBD structures have been obtained in crystal and in solution. The RXRα DBD has been solved in complexes with DNA as homodimers and as heterodimers with the TR DBD and retinoic acid receptor DBD (16–18). The RXR homodimer DBD binds to the DR-1 element as a head to tail dimer. The distance between the DR-1 half-site sequences is ~3 nm, and part of the α-helix connecting DBDs to LBD (T-box) unwinds allowing efficient DNA binding and DBD dimerization (18). RXR LBDs have been crystallized in a variety of forms, including dimers and tetramers (19–23). The LBDs are mostly α-helical with the ligand buried in the interior of the holo-receptor and contributing to formation of the hydrophobic core of the protein. There are significant structural differences between the RXR LBD apo- and holo-forms. In particular, transactivation helix (H12) protrudes from the body of the receptor in the absence of ligand, but packs against the body of receptor in its presence (19, 20, 24, 25). This repositioning of H12 completes formation of a hydrophobic cleft that also contains residues of H3, 4, and 5 and forms a docking site for L*XX*LL motifs in nuclear receptor coactivators. The RXR LBD dimer interface overlaps residues from the intersection of helices 7, 9, and 10 (21) and corresponds to the position of the TR homo- and heterodimerization interface as defined by site-directed mutagenesis (26). A crystal structure of an RXR-LBD tetramer, along with solution x-ray scattering studies of the same oligomer (21, 22), reveals that it consists of a head to head "dimer of dimers" with a large (2750 Å^2) interface comprised of residues from H3, H11, and H12 (discussed further below). This extensive tetramer interface is thought to contribute to the marked stability of this oligomer (27). Comparison of the liganded homodimer structure with the tetramer structure also suggests a reason for the observed ligand-dependent dissociation of tetramers to dimer pairs. Each of the constituent LBDs of the tetramer adopts the typical apo-receptor conformation, in which H12 protrudes from the body of the LBD but then, instead of protruding away from the receptor, actually docks into the H3-H5 hydrophobic cleft region in the adjacent dimer utilizing its LMEML sequence that resembles the coactivator L*XX*LL motif (21). Since ligand repositions H12, addition of ligand to tetramers would be expected to remove this part of the interdimer interface and destabilize the tetramer.

While each of these crystal structures has provided major insights into receptor function, it will be necessary to understand the relationships between distinct receptor domains to completely understand how nuclear receptors work. For example, it is not clear why the RXR dimer binds DR-1 elements with higher affinity than the tetramer. The structures of any nuclear receptor containing multiple domains have not yet been solved. In this study, we report the structural organization of a hRXR protein containing the linked DBD and LBD (hRXR$\alpha\Delta$AB) as revealed by solution synchrotron x-ray scattering studies. We used the available crystallographic structures of the isolated hRXRα DBD and LBD domains to place them inside low resolution *ab initio* small-angle x-ray scattering (SAXS) models, which allowed us to assemble models of both a dimer and a tetramer of hRXR$\alpha\Delta$AB. The results show that the dimer is a U-shaped molecule with the two DBDs in close proximity (2 nM) forming the tips of the U and separated by an angle of 10°. By contrast, the tetramer is a more elongated X-shaped molecule formed by two dimers in head to head arrangement in which the DBDs are extended from the structure and further apart (6 nm) than in the dimer configuration and are separated by an angle of ~30°. These solution structures represent the first x-ray structural studies of nuclear receptors that contain more than one domain and may explain why RXR dimers recognize target genes with higher affinity than tetramers.

MATERIALS AND METHODS

Protein Expression and Purification—The hRXR$\alpha\Delta$AB construct encompassing amino acid residues 126–462 was overexpressed in *Escherichia coli* cells from strain BL21(DE3) harboring a pET28a(+) plasmid (Novagen). A Luria broth (LB) starter culture was inoculated with a single colony of a LB-agar culture and grown overnight at 37 °C. The initial culture was inoculated at 1% in a 2× YT culture (1.6% tryptone, 1% yeast extract, 0.5% NaCl w/v) and grown at 37 °C in 50 μg/ml kanamycin medium until $A_{600\ nm}$ reached 0.8. Then 5 μM of zinc sulfate and 0.5 mM isopropyl-1-thio-β-D-galactopyranoside was added, and the culture was allowed to grow for 2 h of incubation at 37 °C. After this cells were harvested by centrifugation, and the pellets were resuspended in 10 ml/liter culture of buffer A (50 mM sodium phosphate, pH 7.5, 100 mM NaCl, 10% glycerol, 2 mM 2-mercaptoethanol, and 10 mM imidazole). Phenylmethylsulfonyl fluoride and lysozyme were added to 1 mM and 220 μg/ml, respectively, and the culture was placed on ice for 30 min. The lysate was sonicated for six times in 1-min intervals (power 40, Branson Sonifier 450), keeping the culture on ice, and then clarified by centrifugation for 1 h at 20,000 rpm in a Sorval SS34 rotor. The supernatant was loaded onto a 1.5-ml (per liter culture) Talon Superflow Metal Affinity Resin (Clontech) packed in a c10/10 column (Amersham Biosciences) and equilibrated in buffer A (flow rate 70 cm/h). The column was washed with buffer A, until the $A_{280\ nm}$ of the eluent returned to baseline, and then subsequently with buffer B (50 mM sodium phosphate, pH 7.5, 300 mM NaCl, 10% glycerol, 2 mM 2-mercaptoethanol, and 10 mM imidazole). Then, buffer A was applied until the conductivity returned to that expected for the buffer A. The protein was eluted with buffer C (50 mM sodium phosphate, pH 7.5, 100 mM NaCl, 10% glycerol, 2 mM 2-mercaptoethanol, and 300 mM imidazole). Fractions containing hRXR$\alpha\Delta$AB were pooled, diluted 1:1 with a buffer of 10 mM Tris-HCl, pH 7.5, 10% glycerol, 5 mM DTT (dithiothreitol), and 0.5 mM EDTA. The fractions were then loaded onto Q-Sepharose High Performance Resin (7 ml, Amersham Biosciences) and packed in a c10/10 column (Amersham Biosciences) (1 × 10 cm, flow rate 70 cm/h) that had been pre-equilibrated with this same buffer (plus 50 mM NaCl). The column was then washed with 10 ml of a buffer of 10 mM Tris-HCl, pH 7.5, 50 mM NaCl, 10% glycerol, 5 mM DTT, and 0.5 mM EDTA to remove unbound protein and eluted with a gradient of 50–500 mM NaCl. The protein eluted in two peaks, and the fractions of each peak were pooled and concentrated. Protein content and purity of all chromatographic fractions were checked by Coomassie Blue-stained SDS gels. Protein concentrations were determined in parallel using the Bio-Rad dye assay and bovine serum albumin as standard.

Size Exclusion Chromatography and Dynamic Light Scattering Experiments—The protein oligomerization state was assessed by size exclusion chromatography and dynamic light scattering. Each of two protein elution peaks was separately concentrated and loaded onto a Superdex 200 size exclusion column (1 × 30 cm, Amersham Biosciences). The column was pre-equilibrated with a buffer of 10 mM Tris-HCl, pH 8.0, 200 mM NaCl, and 5 mM DTT at a flow rate of 0.5 ml/min and standardized with the molecular mass calibration kit (Amersham Biosciences) using 100 μl of protein standard samples of a known Stokes radii (thyroglobulin, 8.5 nm; ferritin, 6.1 nm; catalase, 5.22 nm; aldolase, 4.81 nm; bovine serum albumin, 3.55 nm; ovalbumin, 3.05 nm; chymotrypsinogen, 2.09 nm, and ribonuclease A, 1.64 nm). The different oligomeric forms of RXR$\alpha\Delta$AB receptor were analyzed under the same conditions. The initial protein concentrations of 2.2, 5.6, and 12.3 mg/ml (peak 1) and 3, 8.2, and 11 mg/ml (peak 2) were studied.

Dynamic light scattering measurements were performed with a DynaPro MS200 instrument (Protein Solutions) at 4 °C using a 12-μl cuvette. The protein samples were concentrated to 1.17 and 7 mg/ml (separately peak 1 and peak 2) in 10 mM Tris-HCl, pH 8.0, 200 mM NaCl, 10% glycerol, and 5 mM DTT prior to measurements.

Small-angle X-ray Scattering Measurements and Data Analysis—SAXS data were collected at the small-angle scattering beamline on the LNLS (National Synchrotron Light Laboratory, Campinas, Brazil) using one-dimensional position-sensitive detector (28). hRXRα at the concentrations 2, 3.1, 6.3, and 14 mg/ml was measured at a wavelength λ = 0.138 nm for sample-detector distances of 632.5 and 1345.2 mm covering the momentum transfer range $0.1 < q < 6$ nm^{-1} ($q = 4\pi\sin\theta/\lambda$, where 2θ is the scattering angle). The scattering curves of the protein solutions and the corresponding solvents were collected in a number of short 30-s to 1-min frames to monitor radiation damage and beam stability. The data were normalized to the intensity of the incident beam and corrected for detector response.

The scattering of the buffer was subtracted, and the difference curves were scaled for concentration. The distance distribution functions p(r) and the radii of gyration R_g were evaluated by the indirect Fourier transform program GNOM (29). The molecular masses of the oligomers of hRXRα in solution were estimated by comparison of the extrapolated forward scattering I(0) with that of a reference solution of bovine serum albumin with a known molecular mass of 66 kDa. Prior to the shape analysis, a constant was subtracted from the experimental data to ensure that the intensity at higher angles decays as q^{-4} following Porod's law for the homogeneous particles (30). The value of the constant is derived automatically from the outer part of the curve by linear fitting in coordinates $q^4I(0)$ *versus* q^4 by the shape determination program DAMMIN (31). This procedure reduces the contribution from scattering due to the internal protein structure and yields an approximation of the "shape scattering" curve (*i.e.* scattering from the excluded volume of particle filled by constant density).

The experimental pair distribution functions do not contain any negative part, which is an indication of the absence of interference effects in the scattering curves produced by spatial correlations. This argues that all solutions were sufficiently dilute to remove interference effects. The structure function that describes interparticle correlations may be equal to unity even at high concentrations for proteins of very anisotropic shape (32).

Shape Determination—Low resolution particle shapes were restored from the experimental SAXS data using two *ab initio* procedures. In the first procedure (33, 34), the shape is represented by an angular envelope function, parameterized in terms of spherical harmonics using multipole expansion methods (35). The maximum number of the spherical harmonics L is selected to keep the number of free parameters $M = (L + 1) - 6$ close to the number of Shannon channels $N_s = D_{max}q_{max}/\pi$ in the experimental data (36).

The computed scattering intensity of the envelope is compared with the experimentally obtained one. The envelope is modified by minimizing the discrepancy χ between the calculated and the experimental data (36, 37). The discrepancy χ is defined in Equation 1,

$$\chi = \sqrt{\frac{1}{N-1}\sum_{j=1}^{N}\left[\frac{I(q_j) - I_{exp}(q_j)}{\sigma(q_j)}\right]^2} \quad \text{(Eq. 1)}$$

where N is a number of the experimental points and $I_{exp}(q_j)$ is the experimental intensity and $\sigma(q_j)$ is its standard deviation in the jth point.

The shapes of the hRXRα dimers and tetramers were also restored from the experimental data using another *ab initio* method as implemented in DAMMIN (31). A sphere of diameter D_{max} was filled by a regular grid of points corresponding to a dense hexagonal packing of small spheres (dummy atoms) of radius $r_0 \ll D_{max}$. The structure of the dummy atom model (DAM) is defined by a configuration X, assigning an index to each atom corresponding to solvent (0) or solute particle (1). The method searches for a compact interconnected configuration X, minimizing the goal function in Equation 2,

$$f(X) = \chi^2 + \alpha P(X) \quad \text{(Eq. 2)}$$

where $\alpha > 0$ is the weight of the looseness penalty (31). Starting from the initial spherical configuration, simulated annealing is employed for the minimization (31).

Both models assume that the protein structure in solution can be described by a constant electron density over its whole volume. However, short range fluctuations in electronic density that exist inside the proteins actually yield a constant contribution at small q. To apply SASHA and DAMMIN this constant contribution should be previously subtracted from the experimental scattering curves. The assumption of a two-electron density model (corresponding to the protein and the solvent) is progressively weaker for increasing q outside the range covered in the present measurements.

The coordinate sets for both hRXRα LBD and DBD domains were obtained from Protein Data Bank (PDB accession numbers 1G1U and 2NLL) (16, 19). Relative positions of the LBD and DBD domains were found by iterative rotation of their envelope functions to minimize the discrepancy with the *ab initio* low resolution structure using an automated procedure. The models were displayed using the program MASSHA (38). Radii of gyration (R_g), maximum intraparticle distances (D_{max}), envelop functions, and scattering curves, were calculated from these atomic coordinates with use of the program CRYSOL taking into account the influence of the hydration shell (39). SUPCOMB (40) was used to superimpose *ab initio* low resolution models with crystallographic structures.

RESULTS

SAXS Measurements of hRXRα DBD-LBD Dimers and Tetramers—The bacterially expressed hRXR$\alpha\Delta$AB preparation eluted from the Q-Sepharose high performance resin ion exchange column in two peaks (1 and 2; see "Material and Methods"). The protein of both chromatographic fractions migrated on SDS-polyacrylamide gels at a molecular weight that is consistent with hRXR$\alpha\Delta$AB region at high purity (>95%; "Material and Methods"). Thus, our preparation of hRXR$\alpha\Delta$AB exists in two distinct forms. To assess the structural organization of the hRXR$\alpha\Delta$AB in solution, separate synchrotron SAXS measurements were performed on each peak. Experimental scattering curves from hRXRα are presented in Fig. 1, and the structural parameters derived from these curves are given in Table I.

The hRXR$\alpha\Delta$AB oligomers eluted in peaks 1 and 2 correspond to molecular masses of 79 and 185 kDa, respectively, as determined in SAXS experiments by comparison with a reference solution of bovine serum albumin (Table I). This suggests that peaks 1 and 2 are composed respectively of hRXR$\alpha\Delta$AB dimers and tetramers. Further support for this finding comes from the size exclusion chromatography analysis (Fig. 2). Peak 1 protein Stokes radius was equal to 4.48 and 4.66 nm at protein concentrations of 5.6 and 12.3 mg/ml, respectively. Peak 2 protein Stokes radius varied from 5.2 to 5.7 nm at several protein concentrations between 3 and 11 mg/ml. Dynamic light scattering experiments conducted on peak 1 and peak 2 fractions at the concentrations 1.2 and 7 mg/ml gave, respectively, experimental Stokes radii of 4.42 and 4.3 nm for peak 1 and 5.13 and 5.42 nm for peak 2. These results are both consistent with the idea that peaks 1 and 2 represent dimer and tetramer, respectively. Determinations of Stokes radius from size exclusion chromatography and dynamic light scattering agree with Stokes radii calculated from proposed low resolution SAXS models of the hRXR$\alpha\Delta$AB dimer and tetramer (see below), which are 4.15 nm for dimer and 5.6 nm for tetramer (41).

Concentration of the protein from peak 1 from 3 to 14 mg/ml yielded SAXS curves that were virtually identical to the SAXS data of the protein from the elution peak 2 at similar concentration (data not shown). This suggests that the hRXR$\alpha\Delta$AB dimer population in peak 1 can be converted to a tetramer population at high protein concentration and is consistent with the previous idea that the DBD-LBD dimer and tetramer populations are in dynamic equilibrium that is influenced by protein concentration (14, 15).

The experimental values of D_{max} and R_g, 19 and 5.27 nm for the tetramer and 11.5 and 3.38 nm for the dimer, respectively, suggest that the protein in both peaks is rather elongated (Table I). The profiles of the distance distribution function p(r) in Fig. 3 are typical for elongated particles (42). Nevertheless, the D_{max} of the tetramer (19 nm) is 7.5 nm larger than the dimer (11.5 nm), which indicates that the tetramer is more elongated than the dimer.

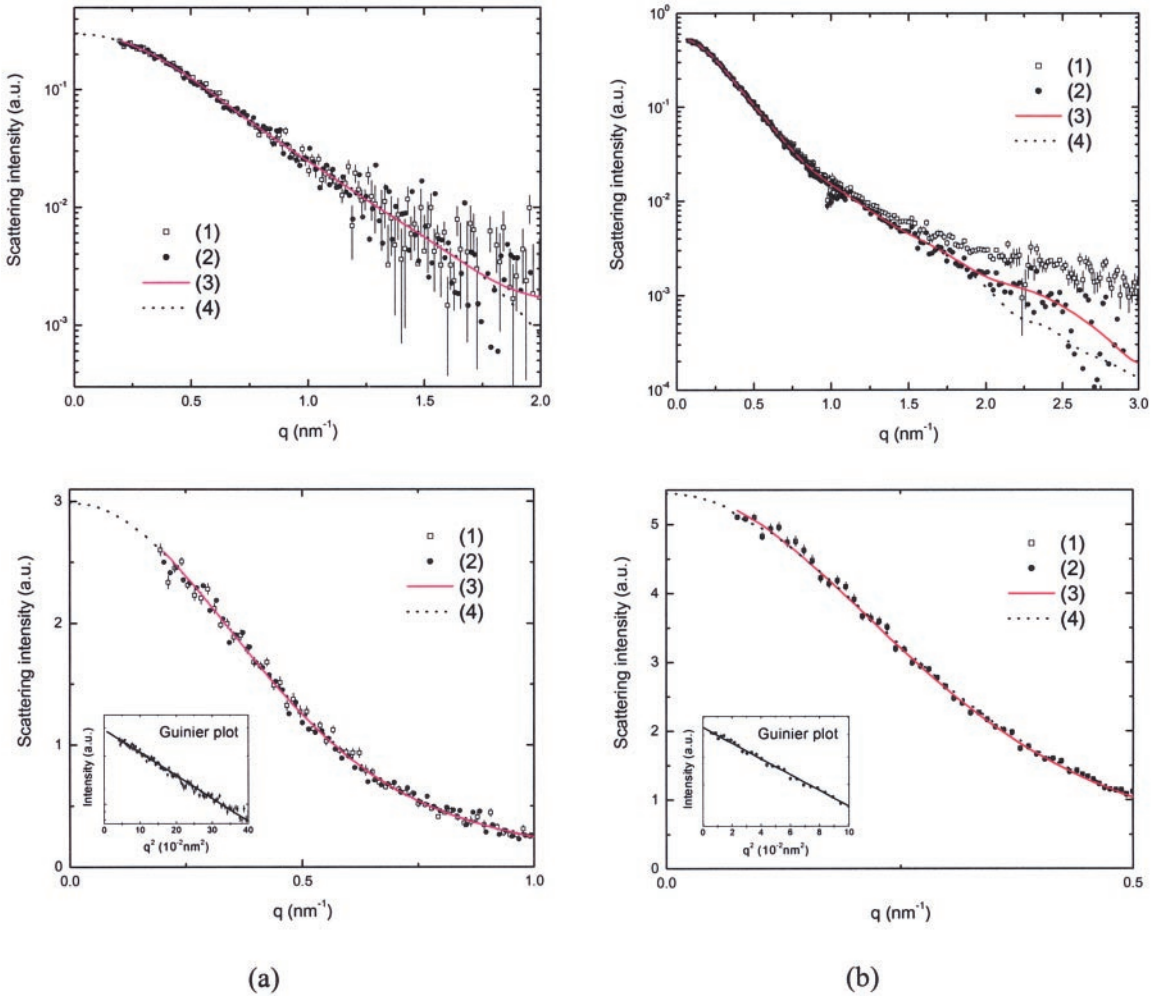

FIG. 1. **Experimental solution scattering curves of hRXRαΔAB and results of the fitting procedures.** *a*, dimer. *b*, hRXRαΔAB tetramer. *Above*, log I *versus q* focusing on the fitting of the experimental curve at high *q*. *Below*, details of the same curve at small *q* in linear scale with an inset containing the correspondent Guinier plots (log I *versus* q^2). (*1*), experimental curve; (*2*) experimental curve after subtraction of a constant value as described under "Materials and Methods"; (*3*) scattering intensity from the DAMs (DAMMIN); (*4*) scattering intensity from the envelope model (SASHA).

TABLE I
Structural parameters derived from SAXS data

Parameter/Sample	hRXR α dimer			hRXR α tetramer		
	Exp.[a]	Env.[b]	DAM[c]	Exp.	Env.	DAM
Mass (kDa)	79 (5)			185 (10)		
D_{max} (nm)	11.5 (5)	12.0	11.0 (2)	19 (1)	20	18 (2)
R_g (nm)	3.38 (5)	3.41	3.36 (1)	5.27 (4)	5.27	5.2 (2)
V (nm^3)	105	151	119 (5)[d]	246	338	285 (3)
Free parameters	6.7[e]	13[d]	2718	14.1[e]	31[f]	3884
Discrepancy χ		0.57	1.32 (1)		0.99	1.30 (2)
Resolution (nm)	3.0	3.3	3.0	1.05	2	2.1

[a] Exp., calculated from the experimental data.
[b] Env., parameters of the envelope models.
[c] DAM, parameters of the dummy atoms models averaged over 10 models.
[d] Symmetry P2 imposed.
[e] Number of Shannon channels is given.
[f] Symmetry P222 imposed.

Ab Initio Shape Determination Using Envelope Functions (SASHA)—Shape determinations of the hRXRα dimer and the hRXRα tetramer were performed using multipole expansion methods. The experimental data were fitted *ab initio* by the scattering from an envelope function starting from a spherical initial approximation (33, 34). The envelopes were represented with spherical harmonics up to $L = 4$ (13 independent parameters) and $L = 10$ (31 independent parameters) for dimer and tetramer, respectively. This was justified by the fact that the portions of the scattering curves used for *ab initio* shape determination using the envelope functions contained $N_s = 6.7$ Shannon channels for hRXRα dimer and $N_s = 14.1$ Shannon channels for hRXRα tetramer. The P2 symmetry was imposed in the case of dimer and P222 in the case of tetramer.

The restored envelope for the dimer is displayed in Fig. 4, and the fits to experimental data presented in Fig. 1. The crystallographic models of hRXRα LBD homodimer and two

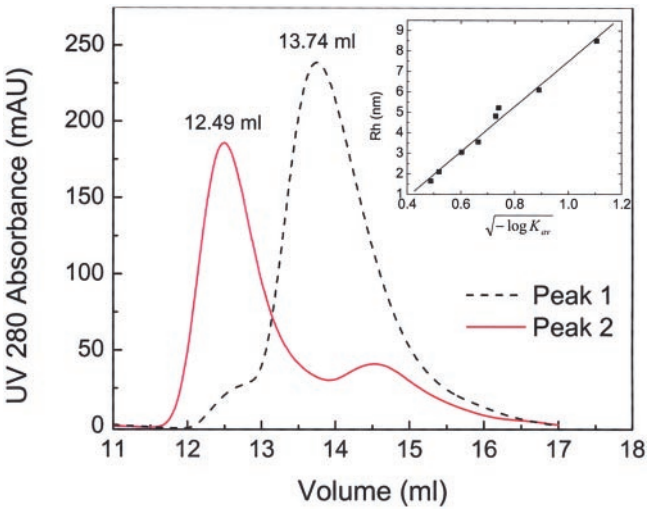

FIG. 2. **Representative size exclusion chromatograms of peak 1 and peak 2 protein fractions.** RXRαΔAB from Q-Sepharose peak 1 and peak 2 elution fractions at initial concentrations of 5.6 and 8.2 mg/ml, respectively, were loaded onto size exclusion Superdex HR200 10/30 column (Amersham Biosciences). Respective elution profiles are shown as a *dashed line* (peak 1) and a *solid line* (peak 2). The value at the top of each peak eluted from size exclusion column corresponds to the elution volume of the RXRαΔAB. The presence of the receptor in these peaks was confirmed by SDS-electrophoresis (data not shown). The elution volumes were used to calculate the K_{av} values (K_{av} = (elution volume − column void volume)/(column total volume − column void volume)). The value of $\sqrt{-log\ Kav}$ was used to determine the Stokes radius for each peak from the column calibration plot (shown as an *inset*). The column calibration plot was obtained eluting the protein standards of known Stokes radii. Thyroglobulin, ferritin, catalase, aldolase, albumin, ovalbumin, chymotrypsinogen, and ribonuclease with the correspondent Stokes radii of 8.5, 6.1, 5.22, 4.81, 3.55, 3.05, 2.09, and 1.64 nm, respectively, were employed.

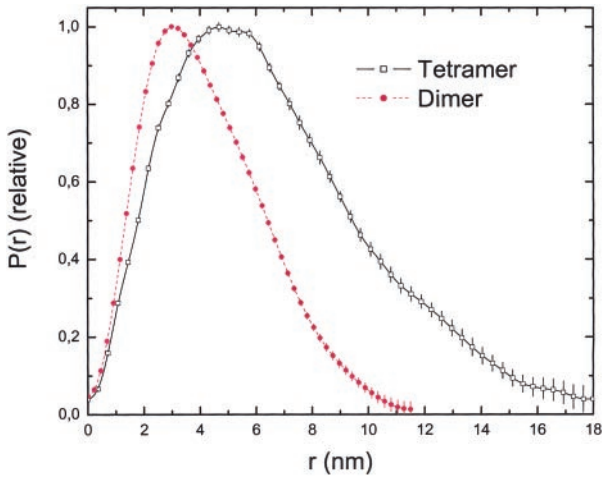

FIG. 3. **Distance distribution functions of the hRXRαΔAB dimer and tetramer.** Distance distribution functions of hRXRαΔAB dimer and tetramer are given in *hollow circles* and *filled circles*, respectively.

hRXRα DBD fragments could be unambiguously positioned inside the envelope for the hRXRα dimer. The restored envelope for the tetramer is displayed in Fig. 5, and fits to the experimental data are displayed in Fig. 1. By contrast to the dimer, one hRXRα LBD tetramer and four hRXRα DBD fragments fit an envelope for the hRXRα tetramer. Two models of the hRXRα LBD dimers obtained by superposition of the crystallographic structures with *ab initio* hRXRα dimer structure were placed within the tetramer *ab initio* models allowing for their relative rotation and translation around common 2-fold axis and adjustment of a relative orientation of the DBDs. This superposition fits the *ab initio* retrieved low resolution tetramer structure. Stokes radii calculated on the basis of retrieved low resolution structures of dimer and tetramer is equal to 4.15 and 5.6 nm, respectively (41). These values agree with experimental values observed for dimer and tetramer populations in size exclusion chromatography and dynamic light scattering.

Ab Initio Shape Determination Using DAM Technique (DAMMIN)—The particle shapes were also computed by the second *ab initio* procedure using the DAMMIN program (31). In this method, a sphere of diameter D_{max} is filled with densely packed small spheres (dummy atoms) with radius $r_0 \ll D_{max}$. The method searches to minimize differences between experimentally determined scattering curves and those calculated from DAM models using simulated annealing algorithm. The "looseness" penalty term ensures that the procedure yields a compact and interconnected model. The models were derived from the experimental data assuming a 2-fold symmetry for the dimer and p222 symmetry for the tetramer. The symmetry restrictions resulted in a significant reduction in the number of free parameters of the models. The search volume for hRXRα dimer has been filled with N_{DAM} = 2718 dummy atoms with a packing radius r_a = 0.375 nm within a sphere with the diameter D_{max} = 11.5 nm. The search volumes for hRXRα tetramer have been filled with N_{DAM} = 3884 dummy atoms with a packing radius r_a = 0.575 nm within a sphere with the diameter D_{max} = 20.0 nm. Forty independent *ab initio* simulations were performed. Of those, 395 ± 10 dummy atoms were attributed to the final model of hRXRα dimer, and 265 ± 5 atoms were assigned to the final model of the hRXRα tetramer.

The obtained DAMs are presented in Figs. 4 and 5. DAM-derived structure parameters also agree with the experimental values (Table I). To verify the uniqueness of the shape restoration using DAM, several independent restorations were performed using different starting conditions yielding reproducible results. Maximum concentrations of the protein used for SAXS solution studies of the hRXRα dimer (3.1 mg/ml) and the hRXRα tetramer (14 mg/ml) limited the maximum resolution of the final models to 3.0 and 2.1 nm, respectively (Table I). These resolutions do not permit unambiguous determination of the spatial positions of their secondary structure elements, but allowed us to obtain the overall shape of the molecules and relative position of their individual domains

hRXRα Dimer and Tetramer Solution Structure—The best fitting SAXS hRXRαΔAB dimer model, constructed as described in the preceding two sections, is shown in Fig. 4. The dimer is an anisometric U-like-shaped molecule with two clearly developed substructures that correspond to homodimers of the LBD and DBD. The two LBDs form the plate-like base of the U, and each LBD is connected by a long α-helical peptide, protruding like an arm, to its DBDs placed at the extreme of the U (Fig. 4). The LBDs dimerize through the interface described in the hRXRα crystal structure (19, 20), involving contacts between H9 and H10. The two long α-helices connecting LBDs to DBDs are slightly twisted around the 2-fold symmetry axis of the molecule. The DBDs form an angle of ~10 degrees in and out of plane of the LBDs but adopt a position that is relatively close together in a head to head orientation. The distance between the DBDs in solution is slightly over 2 nm, which is comparable to the distance between half-sites of a DR-1 element (3 nm). However, since these are placed in a head to head orientation, rotation of one of the DBDs by about 180° would be required for the homodimer to bind to a DR-1 element. Assuming that this rotation could occur, the data are consistent with the notion that the

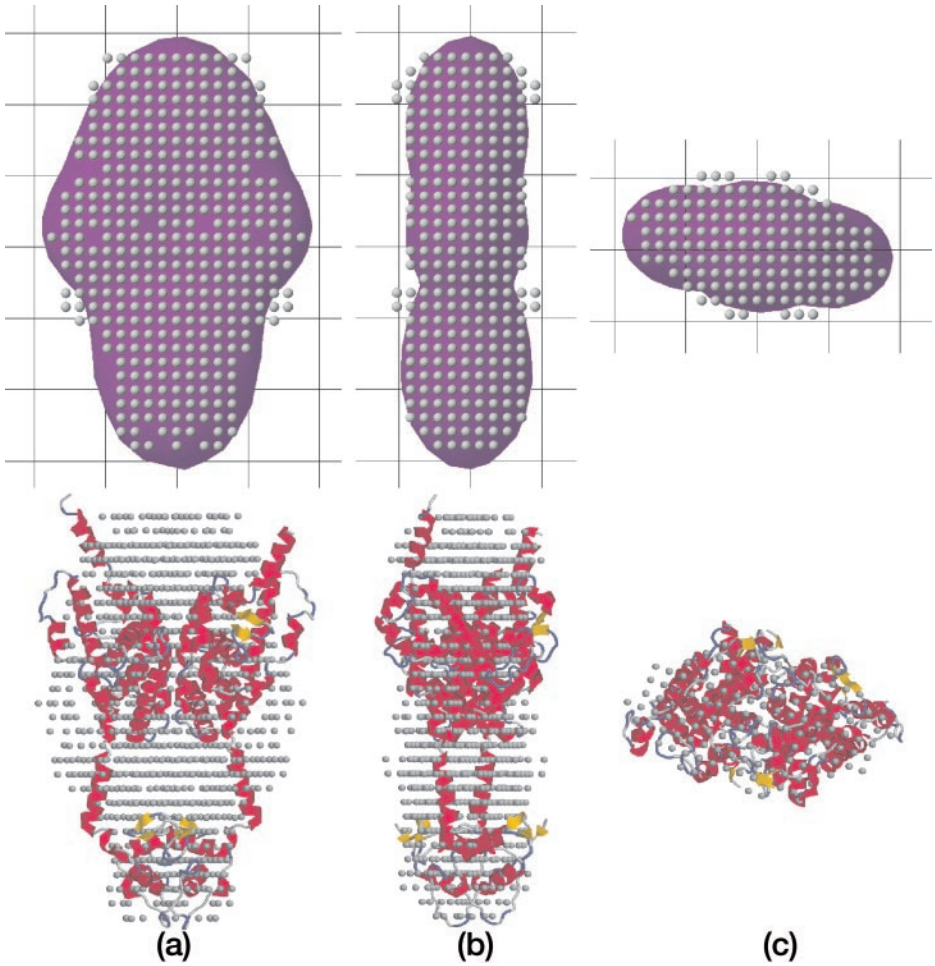

FIG. 4. **SAXS hRXR$\alpha\Delta$AB dimer envelopes derived from *ab initio* calculations.** *a*, *upper row* shows a superposition of the envelop model computed by SASHA (34) to the average of ten DAMs obtained by DAMMIN (31), and the *lower row* represent the superposition of the same ten DAMs to the x-ray structure of the hRXRα LBD dimer (21) and two hRXRα DBDs (23). Grid space is 2 nm. *b* and *c* are the same model rotated counterclockwise by 90° around the *z*- and *y*-axes, respectively.

hRXR$\alpha\Delta$AB homodimer that we observe in solution is capable of binding to its cognate DNA response element.

The hRXRα tetramer is an oblate and more elongated X-shaped molecule (Fig. 5 and Table I). Like the dimer, the tetramer contains well developed substructures that correspond to the LBDs and DBDs (Fig. 5). However, in the tetramer, the LBDs comprise the center of the molecule and the four DBDs protrude from the center. The relative position of the LBDs is consistent with previous crystallographic and solution studies of the hRXRα LBDs, which show that the tetramer is composed of a dimer of dimers where the LBDs of one dimer are in head to head arrangement with the LBDs of the other dimer. To fit better experimental scattering curves we allowed for relative rotation of homodimers around their 2-fold symmetry axis and for adjustment of the distance between their centers of masses. The model is consistent with the idea that individual dimer pairs utilize the previously defined interface that overlaps the intersection of H9 and H10 and that the extensive tetramerization interface utilizes interactions between H3-H3, H11-H11, and H12 with the H3-H5 hydrophobic cleft region in the adjacent dimer (21), although limited resolution of SAXS models does not allowed detailed description (Fig. 5). However, in striking contrast to the DBD-LBD homodimers, the DBDs of the tetramer were not close together (Figs. 4 and 5). Individual distances between the DBDs of each dimer pair were 6 nm. This suggests that the DBDs of the RXR tetramer would not be able to interact with the DR-1 element without significant conformational changes. Thus, the x-ray solution studies of the RXR tetramer present an explanation why it may not bind well to DNA.

DISCUSSION

Small-angle x-ray scattering analyses yield data that permits assembly of structural models of protein in solution. The technique has some obvious disadvantages, especially relative to x-ray crystallography. First, the data is collected at relatively low resolution (nm range relative to angstrom range) and therefore does not permit accurate determinations of the position of individual amino acids and their side chains within the structure. Second, the technique relies on modeling of relatively low amounts of data and therefore depends upon assumptions about the tertiary and quaternary structure of the protein and internal symmetries of the overall structure (see "Materials and Methods"). Should these assumptions prove incorrect, then the deduced structures may prove to be inaccurate. Nevertheless, the technique is useful for less detailed descriptions of overall protein conformations and, further, can be used in conjunction with published high resolution crystal structures to infer the likely conformation of proteins in solution. In this sense, small-angle scattering may have some advantages over x-ray crystallography, which provides a high resolution "snapshot" of a particular conformation within a crystal lattice, which might be influenced by the crystal packing and can not always be readily interpreted in terms of the oligomeric units of the protein in solution.

In this study, we reported low resolution synchrotron small-angle scattering structures of unliganded hRXR$\alpha\Delta$AB oligomers. We employed two independent *ab initio* shape restoration methods to obtain a molecular envelope of RXRα in its dimeric and tetrameric forms to 3.0 and 2.1 nm, respectively. The two *ab initio* shape restoration methods differ in that

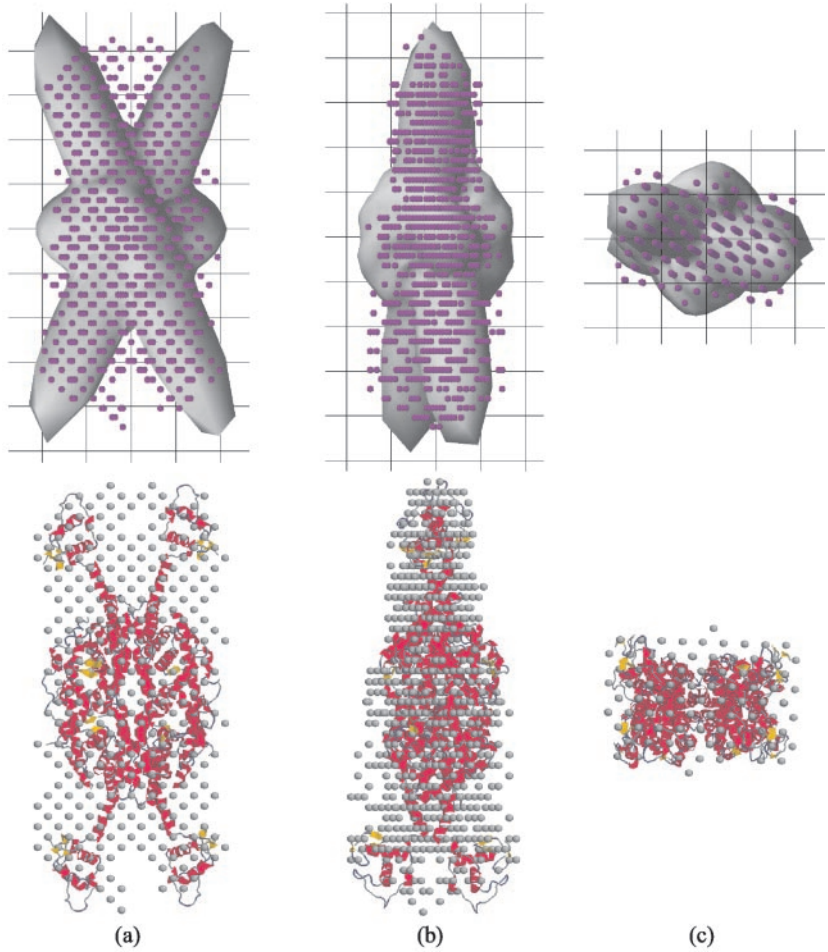

FIG. 5. **SAXS hRXRαΔAB tetramer models obtained by two independent *ab initio* approaches.** *a*, *upper row* shows a superposition of the envelop model obtained by SASHA (34) to the average of ten DAM calculated by DAMMIN (31), and the *lower row* represents the superposition of the same ten DAM to the x-ray structure of the hRXRαΔ LBD tetramer (21) and four hRXRα DBDs (23). Grid space is 2 nm. *b* and *c* are the same model rotated counterclockwise by 90° around the *z*- and *y*-axes, respectively.

SASHA modeling yields an overall molecular envelope, whereas DAMMIN modeling provides a dummy atoms model. Figs. 4 and 5 demonstrate that the dummy atoms derived from the DAMMIN model are highly dense inside the envelope derived from the SASHA model, whereas density of dummy atoms outside it is low. Given the differences in the number of adjustable parameters (Table I), the methods therefore agree well within the limits imposed by the intrinsically low resolution of SAXS. Our models for dimer and tetramer forms indicate that both oligomers are relatively elongated and further suggest that the dimer adopts an oblate conformation, whereas the tetramer adopts an X-shaped conformation. The Stokes radii computed on the basis of the proposed low resolution models for both oligomers agrees well with the experimental measurements of Stokes radii independently obtained by size exclusion chromatography and dynamic light scattering studies (see "Results"), providing independent biochemical verification of our models.

In an attempt to understand the divergent nature of the dimer and tetramer shapes, we positioned published crystallographic models of the hRXRα DBD fragment (23) and hRXRα LBD homodimers/homotetramers (21) within the *ab initio* dimer and tetramer structures. Internal P2 and P222 symmetries were imposed in the case of the dimer and the tetramer, respectively (Figs. 4 and 5). These symmetries correspond to the internal symmetry of the previously determined RXRα LBD crystal structure (21) and were also previously confirmed by solution scattering studies of the same LBD protein (20). Given these constraints, the crystallographic models show a relatively good fit into the dimer and tetramer envelopes. The likeliest hRXRαΔAB dimer conformation is a U-shaped structure with the two DBDs occupying the tips of both arms of the U. The DBDs are closely positioned in such a way that they could contact DNA without major conformational changes of the protein. However, as discussed in the Introduction, RXR homodimers preferentially bind to DR-1 elements containing DNA half-sites spaced as direct repeats. Thus, if the LBDs are dimerized as shown in this structure and by mutational analyses one of the DBDs would have to rotate by ~170–180° for the homodimer to bind to DNA. Alternatively, the DBD-LBD conformation that is revealed in this structure could bind DNA if one of the DBDs were to bind nonspecifically to one of the half-sites. By contrast, the hRXRαΔAB tetramer adopts an X-shaped structure in solution. The LBDs are known to tetramerize by forming a head to head arrangement of paired dimers (dimer of dimers) with extensive contacts between H3-H3, H11-H11, and H12 with the coactivator cleft of the neighboring molecule. The likeliest tetramer structure fits the head to head arrangement of LBD homodimers into the middle of the X shape, and the DBDs would occupy the tips of the four points. Interestingly, the DBDs of the tetramer would be widely spaced in this configuration and therefore unlikely to bind DR-1 elements with high affinity without major conformational changes. Thus, we propose that the dimeric and tetrameric forms of the LBD differentially position the RXR DBDs, suggesting that RXR tertiary structure is sensitive to alterations in its quaternary state. These low resolution structures represent the first models proposed for a nuclear receptor containing both a DBD and LBD. Moreover, our models suggest an explanation for the observed inability of the unliganded tetramer to bind to DNA.

Although these results cannot absolutely assure that other

models would not give a better fit, we believe that the obtained solutions must be close to reality. First, the molecular envelopes obtained by two independent shape restoration methods (SASHA and DAMMIN) give similar solutions and the deduced Stokes radii from the models correspond well to the observed Stokes radii. Second, the DBD and LBD crystal structures fit well into the overall molecular envelopes. Third, the maximum dimensions retrieved from the p(r) function impose rather elongated shapes that are hard to explain by alternative placements of RXR LBDs and DBDs without invoking conformations that contradict previous results from high resolution crystallography and molecular genetics. Nevertheless, while the majority of dummy atoms derived from the DAMMIN modeling technique fit into the molecular envelope derived from the SASHA modeling technique, we recognize that there are discrepancies in the placement of some DAMs (Figs. 4*a* and 5*a*). These differences could reflect a natural level of error in modeling techniques or uncertainties in the structure of the molecule in solution at these locations. We can not distinguish these possibilities, but it is interesting that the greatest disagreements in the dimer structure lie around the upper part of the LBD around the predicted position of H12 and the greatest disagreements in the tetramer structure lie close to the predicted position of the DBDs. It is intriguing to suggest that these discrepancies between techniques may reflect relative mobility of these regions of the protein in solution.

While solution x-ray studies can tell us that the relative orientation of the LBD and DBD may differ in the dimer and tetramer forms, the relatively low resolution of the structures prevents us from learning why. We suggest that differences in the conformation of the LBDs in the dimer and tetramer form alter the relative position of the H1/hinge region and reposition the DBDs. However, these subtle changes, if they exist, would be too small to be perceived in solution x-ray scattering. Nonetheless, we note that several distinct lines of evidence indicate that nuclear receptor LBDs must be able to influence the behavior of the DBD. For instance, RXR homodimer binding to DR-1 elements is enhanced by hormone. Thus, ligand-induced conformational changes in the LBD must improve the fit between hRXR and DR-1 and increase the affinity of the interaction. Likewise, TR homodimer binding to DR-4 and to an inverted palindromic element (F2) is reduced by hormone (43–45). In the case of TR homodimers, we hypothesize that ligand-induced conformational changes alter the relative position of the TR DBDs and thus reduce the fit of the TR for both types of response element. It will be important to obtain crystal structures of liganded nuclear receptors containing more than one domain and bound to a variety of DNA elements to understand these phenomena.

The dynamic equilibrium between RXR oligomers is influenced by receptor concentrations, ligand, and DNA (14, 15). Thus, it seems plausible that sequestration of RXR in tetramers *in vivo* could provide a mechanism for the cell to store an excess of receptors until physiological functions related to RXR homodimer and heterodimer activities are called into action (14, 15). In addition to the inactivation revealed by the current studies through separation of the RXR DBDs, a second mechanism for inactivation is provided by structural studies of the RXR LBD tetramer (21). In this case, H12 of one receptor binds to the H3-H5 region of the neighboring molecule, an interaction that is partially analogous to the way that coactivator peptides bind to the nuclear receptor hydrophobic cleft. Placement of H12 from one receptor into the H3-H5 region of the other receptor prevents coactivator binding by occluding the hydrophobic cleft. Our recent studies revealed that the TR and RXR hydrophobic cleft also binds the corepressor N-CoR, suggesting that the orientation of H12 in the tetramer could also occlude the RXR N-CoR interaction surface (46).

While our studies have uncovered possible structures of the unliganded hRXR$\alpha\Delta$AB tetramer, RXR may also be able to form biologically active tetramers in a different configuration. The cellular retinol-binding protein II (CRBPII) promoter contains two non-optimal DR-1 sites that are poorly recognized by the RXR dimer, suggesting that the RXR tetramer is the active species for controlling expression of CRBPII (47–49). These data argue that RXR tetramers control gene regulation *in vivo* through cooperative DNA binding to the CRBPII promoter (47) and to a wide variety of four differently oriented half-sites both *in vitro* and *in vivo* (49). While the interactive surfaces leading to the formation of this type of tetramer are also located in the LBD (49), it is likely that this tetramer is different from the one that we have described here because hormone-dependent activation of CRBPII gene expression will require coactivator recruitment, which as discussed above would be excluded in the tetramer structure that was used to obtain the model in the current studies. We also stress that our studies exclude the RXR N-terminal domain. RXRα or RXRγ, but not RXRβ, can form tetramers cooperatively on the CRBP-II promoter and regulate this gene efficiently (49), and the differences between the isoforms maps to the RXRβ N-terminal domain. This suggests the RXR N-terminal domain may play an important role in regulating formation of the active DNA and ligand-dependent tetramer.

In conclusion, the low resolution solution structures for the hRXR$\alpha\Delta$AB region determined in this work provides the first three-dimensional model for the member of the nuclear receptor super family containing more then one functional domain. Our studies suggest a possible explanation for the previously observed differences in DNA binding activity between dimers and tetramers. The present *ab initio* models of hRXRα dimer and hRXRα tetramer also provide a basis for further analysis of the hRXRα interaction with ligands and DNA response elements.

REFERENCES

1. Maglich, J. M., Sluder, A., Guan, X., Shi, Y., McKee, D. D., Carrick, K., Kamdar, K., Willson, T. M., and Moore, J. T. (2001) *Genome Biol.* **2,** 1–7
2. Evans, R. M. (1988) *Science* **240,** 889–895
3. Lazar, M. A. (1993) *Endocr. Rev.* **14,** 184–193
4. Ribeiro, R. C. J., Apriletti, J. W., Wagner, R. L., West, B. L., Feng, W., Huber, R., Kushner, P. J., Nilsson, S., Scanlan, T. S., Fletterick, R. J., Schaufele, F., and Baxter, J. D. (1998) *Rec. Prog. Horm. Res.* **53,** 351–394
5. Tsai, M. J., and O'Malley, B. W. (1994) *Ann. Rev. Biochem.* **63,** 451–486
6. Horwitz, K. B., Jackson, T. A., Rain, D. L., Richer, J. K., Takimoto, G. S., and Tung, L. (1996) *Mol. Endocrinol.* **10,** 1167–1177
7. Sporn, M. B., Roberts, A. B., and Goodman, D. S. (eds) (1994) *The Retinoids: Biology, Chemistry, and Medicine*, Raven Press, Ltd., New York
8. Mangelsdorf, D. J., and Evans, R. M. (1995) *Cell*, **83,** 841–850
9. Kastner, P., Mark, M., and Chambon, P. (1995) *Cell*, **83,** 859–869
10. Chawla, A., Repa, J. J., Evans, R. M., and Mangelsdorf, D. J. (2001) *Science*, **294,** 1866–1870
11. Mukherjee, R., Strasser, J., Jow, L., Hoener, P., Paterniti, J. R., Jr., and Heyman, R. A. (1998) *Arterioscler. Thromb. Vasc. Biol.* **18,** 272–276
12. de Urzula, A. M., Liu, S., Sjoberg, M., Zetterstrom, R. H., Griffiths, W., Sjovall, J., and Perlmann, T. (2000) *Science*, **290,** 2140–2144
13. Mukherjee, R., Davies, P. J. A., Crombie, D. L., Bischoff, E. D., Cesario, R. M., Jow, L., Hamann, L. G., Boehm, M. F., Mondon, C. E., Nadzan, A. M., Paterniti, J. R., and Heyman, R. A. (1997) *Nature* **386,** 407–410
14. Kersten, S., Pan, L., Chambon, P., Gromemeyer, H., and Noy, N. (1995) *Biochemistry* **34,** 13717–18721
15. Chen, Z.-P., Iyer, J., Bourguet, W., Held, P., Mioskowski, C., Lebeau, L., Chambon, P., and Gromemeyer, H. (1998) *J. Mol. Biol.* **275,** 55–65
16. Rastinejad, F., Wagner, T., Zhao, Q., and Khorasanizadeh, S. (2000) *EMBO J.* **19,** 1045–1054
17. Zhao, Q., Khorasanizadeh, S., Miyshi, Y., Lazar, M. A., and Rastinejad, F. (1998) *Mol. Cell* **1,** 849–861
18. Zhao, Q., Chasse, S. A., Devarakonda, S., Sierk, M. L., Ahvazi, B., and Rastinejad, F. (2000) *J. Mol. Biol.* **296,** 509–520
19. Bourguet, W., Ruff, M., Chambon, P., Gronemeyer, H., and Moras, D. (1995) *Nature* **375,** 377–382
20. Egea, P. F., Mitschler, A., Rochel, N., Ruff, M., Chambon, P., and Moras, D. (2000) *EMBO J.* **19,** 2592–2601
21. Gampe, R. T., Jr., Montana, V. G., Lambert, M. H., Wisely, G. B., Milburn, M. V., and Xu, H. E. (2000) *Genes Dev.* **14,** 2229–2241

22. Egea, P. F., Rochel, N., Birck, C., Vachette, P., Timmins, P. A., and Moras, D. (2001) *J. Mol. Biol.* **307,** 557–576
23. Rastinejad, F., Perlmann, T., Evans, R., and Sigler, P. B. (1995) *Nature* **375,** 203–211
24. Wurtz, J.-M., Bourguet, W., Renauld, J.-P., Vivat, V., Chambon, P., Moras, D., and Gronemeyer, H. (1996) *Nat. Struct. Biol.*, **3,** 87–94
25. Moras, D., and Gronemeyer, H. (1998) *Curr. Opin. Cell Biol.*, **10,** 384–391
26. Ribeiro, R. C. J., Feng, W., Wagner, R. L., Costa, C. H. R. M., Pereira, A. C., Apriletti, J. W., Fletterick, R. J., and Baxter, J. D. (2001) *J. Biol. Chem.* **276,** 14987–14995
27. Kersten, S., Pan, L., and Noy, N. (1995) *Biochemistry*, **34,** 14263–14269
28. Kellermann, G., Vicentin, F., Tamura, E., Rocha, M., Tolentino, H., Barbosa, A., *et al.* (1997) *J. Appl. Crystallogr.* **30,** 880–883
29. Svergun, D. I. (1992) *J. Appl. Crystallogr.* **25,** 495–503
30. Porod, G. (1982) in *Small-angle X-ray Scattering* (Glatter, O., and Kratky, O., eds) pp. 17–51, Academic Press, London
31. Svergun, D. I. (1999) *Biophys. J.* **76,** 2879–2886
32. Guinier, A., and Fournet, G. (1955) *Small-angle Scattering of X-rays*, John Wiley & Sons, NY
33. Svergun, D. I., Volkov, V. V., Kozin, M. B., and Sturmann, H. B. (1996) *Acta Crystallogr. Sect. A* **52,** 419–426
34. Svergun, D. I., Volkov, V. V., Kozin, M. B., Sturmann, H. B., Barberato, C., and Koch, M. H. J. (1997) *J. Appl. Crystallogr.* **30,** 798–802
35. Sturmann, H. B. (1970) *J. Phys. Chem.* **72,** 177–182
36. Shannon, C. E., and Weaver, W. (1949) *The Mathematical Theory of Communication*, University of Illinois Press, Urbana, IL
37. Svergun, D. I., and Stuhrmann, H. B. (1991) *Acta Crystallogr. Sect. A.* **47,** 736–744
38. Konarev, P. V., Petoukhov, M. V., and Svergun, D. I. (2001) *J. Appl. Crystallogr.* **34,** 527–532
39. Svergun, D. I., Barberato, C., and Koch, M. H. (1995) *J. Appl. Crystallogr.* **28,** 768–773
40. Kozin, M. B., and Svergun, D. I. (2001) *J. Appl. Crystallogr.* **34,** 33–41
41. Garcia de la Torre, J., Huertas, M. L., and Carrasco, B. (2000) *Biophys. J.* **78,** 719–730
42. Feigin, L. A., and Svergun, D. I. (1987) *Structure Analysis by small-angle X-ray and Neutron Scattering*, pp. 83–87, Plenum Press, New York
43. Ribeiro, R. C., Kushner, P. J., Apriletti, J. W., West, B. L., and Baxter, J. D. (1992) *Mol. Endocrinol.* **6,** 1142–1152
44. Yen, P. M., Darling, D. S., Carter, R. L., Forgione, M., Umeda, P. K., and Chin, W. W. (1992) *J. Biol. Chem.* **267,** 3565–3568
45. Ribeiro, R. C., Apriletti, J. W., Yen, P. M., Chin, W. W., and Baxter, J. D. (1994) *Endocrinology* **135,** 2076–2085
46. Marimuthu, A., Feng, W., Tagami, T., Nguyen, H., Jameson, L. J., Fletterick, R. J., Baxter, J. D., and West, B. L. (2002) *Mol. Endocrinol.* **16,** 271–286
47. Mangelsdorf, D. J., Umensono, K., Kliewer, S. A., Borgmeyer, U., Ong, E. S., and Evans, R. M. (1991) *Cell* **66,** 555–561
48. Chen, H., and Privalsky, M. L. (1995) *Proc. Natl. Acad. Sci.* **92,** 422–426
49. Lin, B. C., Wong, C. W., Chen, H. W., and Privalsky, M. L. (1997) *J. Biol. Chem.* **272,** 9860–9867